

- Reaction $C_2H_6^+ \rightarrow C_2H_4^+ + H_2$. *Org. Mass Spectrom.* **1993**, *28*, 1262–1269.
- (18) Weitzel, K. M. Tunneling RRKM Calculations for the H_2 Loss Reaction from Ethane Ions on an *ab Initio* Potential Energy Surface. *Int. J. Mass Spectrom. Ion Proc.* **1994**, *136*, 1–24.
- (19) Lifshitz, C. Tropylium Ion Formation from Toluene: Solution of An Old Problem in Organic Mass Spectrometry. *Acc. Chem. Res.* **1994**, *27*, 138–144.
- (20) Duffy, L. M.; Keister, J. W.; Baer, T. Isomerization and Dissociation in Competition: The Pentene Ion Story. *J. Phys. Chem.* **1995**, *99*, 17862–17871.
- (21) Oblinger, M.; Lorquet, A. J.; Lorquet, J. C. *Ab Initio* Study of the Reaction $C_2H_4^+ \rightarrow C_2H_3^+ + H$. *Int. J. Mass Spectrom. Ion Proc.* **1997**, *167/168*, 149–160.
- (22) Mazyar, O. A.; Baer, T. Isomerization and Dissociation in Competition: The Two-component Dissociation Rates of Energy-selected Methyl Formate Ions. *J. Phys. Chem. A* **1998**, *102*, 1682–1690.
- (23) Uzer, T. Theories of Intramolecular Vibrational Energy Transfer. *Phys. Rep.* **1991**, *199*, 73–146.
- (24) Wyatt, R. E.; Zhang, J. Z. H., Eds. *Dynamics of Molecules and Chemical Reactions*; Marcel Dekker: New York, 1996.
- (25) Gruebele, M. Vibrational Energy Flow: A State Space Approach. *Adv. Chem. Phys.* **2000**, *114*, 193–261.
- (26) Chesnavich, W. J.; Bowers, M. T. Theory of Ion–neutral Interactions: Application of Transition-state Theory Concepts to both Collisional and Reactive Properties of Simple Systems. *Prog. React. Kinet.* **1982**, *11*, 137–267.
- (27) Robertson, S.; Wagner, A. F.; Wardlaw, D. M. Flexible Transition-state Theory for a Variable Reaction Coordinate: Derivation of Canonical and Microcanonical Forms. *J. Chem. Phys.* **2000**, *113*, 2648–2661.
- (28) Quack, M.; Troe, J. Specific Rate Constants of Unimolecular Processes. II. Adiabatic Channel Model. *Ber. Bunsenges. Phys. Chem.* **1974**, *78*, 240–252.
- (29) Troe, J. Specific Rate Constants $k(E, J)$ for Unimolecular Bond Fissions. *J. Chem. Phys.* **1983**, *79*, 6017–6029.
- (30) Troe, J. Statistical Adiabatic Channel Model for Ion–Molecule Capture Processes. *J. Chem. Phys.* **1987**, *87*, 2773–2780.

J. C. Lorquet and B. Leyh*
Université de Liège, Belgium

*Research associate of the F.N.R.S. (Belgium)

Kinetic Energy Release Distributions in Mass Spectrometry

1. Introduction

To achieve a detailed understanding of a reaction taking place in a mass spectrometer many complementary experiments have to be performed and analyzed. The reactant and product structures have to be firmly established, the reaction thermochemistry must be measured, along with the microcanonical (or sometimes canonical) rate constant. In addition to these investigations, a further measurement can be carried out to answer the following

question. How does the energy in excess of the thermochemical threshold for a dissociation reaction distribute between the available degrees of freedom of the fragments?

Statistical theories have been widely used to calculate rate constants and energy distributions of the fragments (1–4). These theories assume a complete internal energy randomization before dissociation takes place. They require that the rate of intramolecular energy redistribution be large compared with the dissociation rate. The system has then reached a microcanonical equilibrium. The rate constant formula emerging from the Rice-Ramsperger-Kassel-Marcus (RRKM) or Quasi-Equilibrium (QET) theories shows that two regions of the potential energy surface are relevant: the reactant region and the transition state (see *Theory (Reactions): Statistical Theories in Mass Spectrometry*). In a first approach, the choice of the transition state is straightforward when a saddle point appears along the reaction path. This is usually the case for an early, also called tight, transition state, whose geometry is akin to the reactant molecular ion, or to a reacting intermediate if a multistep reaction is considered. This involves necessarily a maximum of the potential energy along the reaction coordinate and therefore a so-called reverse activation barrier, i.e., a barrier for the reverse association reaction. A statistical calculation of the rate constant in the absence of a saddle point—i.e., in the case of a loose transition state—is not straightforward and alternative solutions, such as the variational transition state theory have then to be applied (see *Theory (Reactions): Statistical Theories in Mass Spectrometry*). On the contrary, the energy distribution of the reaction fragments is mainly governed by another part of the potential energy surface, namely the fragment region. As far as statistical approaches are concerned, rate constants and energy distributions behave quite differently. RRKM calculations work better for tight transition states, whereas the fragment energy distributions for many reactions proceeding through loose transition states have been found to agree fairly well with statistical approaches that assume that all exit channels are equally probable when, in addition, energy and momentum conservation laws are taken into account. In the presence of a reverse activation barrier, however, dynamical interactions between the receding fragments are significant and the purely statistical theories are no longer appropriate. To summarize: (i) both the rate constant and the energy partitioning are essential probes into the potential energy surface governing the reaction; and (ii) some insight can be gained by comparing the predictions of a statistical theory with the experimentally determined energy distributions. As a matter of fact, it can be shown that the fragment energy distributions are much more sensitive to any deviation from the statistical hypotheses than the rate constant (4).

2. Kinetic Energy Release Distributions of Fragment Ions (KERD)

The energy in excess of the thermochemical threshold for a dissociation reaction can be partitioned among all the degrees of freedom of the fragments (see *Ion Spectroscopy: Product State Distributions*). The latter include the relative translation of the receding particles as well as the rotational, vibrational, and possibly electronic motions associated with each fragment (Fig. 1).

A complete characterization of the energy partitioning would require determining a very cumbersome probability distribution,

$$P(\varepsilon, E_r, E_v, E_{el}|E)$$

where E is the excess energy with respect to the dissociation asymptote, E_r , E_v , and E_{el} are, respectively, the rotational, vibrational, and electronic energy of the fragments, and ε is the relative translational energy. Except for very simple, mostly triatomic systems, this complete information is not available experimentally. One must focus instead on a specific degree of freedom. In mass spectrometric experiments, the distribution of the relative translational energy of the receding fragments is the accessible observable (*1, 5*). It can be defined as follows:

$$P(\varepsilon|E) = \int_0^{E-\varepsilon} dE_r \times \int_0^{E-\varepsilon-E_r} dE_v P(\varepsilon, E_r, E_v, E_{el} = E - \varepsilon - E_r - E_v|E) \quad (1)$$

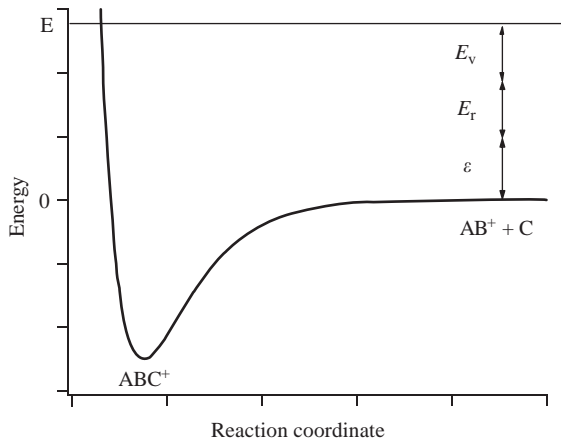


Figure 1

Energy disposal in the unimolecular dissociation of a polyatomic ion.

More simply, the translational energy distribution of the fragments results from the integration over all degrees of freedom that are not measured in the experiment. This distribution is usually referred to as the “kinetic energy release distribution” of the fragments or even more briefly under the acronym KERD. The notation $P(\varepsilon|E)$ is to be read “the probability of releasing a relative translational energy ε if the total internal energy is E ”.

The next section will be devoted to the experimental methods available to determine such KERDs, but before addressing this question, we shall become familiar with the concept by considering a first example and comparing it with a statistical estimate. Let us consider a simple bond cleavage, such as the $C_6H_5I^+ \rightarrow C_6H_5^+ + I$ dissociation, characterized by a monotonic increase of the potential energy along the reaction coordinate, such as the situation depicted in Fig. 1. When this reaction is studied in the microsecond time frame, an appropriate handling of the experimental data leads to a kinetic energy release distribution such as the one displayed in Fig. 2. This KERD resembles more or less a Boltzmann distribution, with an initial steep rise followed by a maximum and an exponential decay at higher kinetic energies. Now, how does this compare with a statistical calculation? As we shall see later, several approaches are possible. Let us start from the simplest possible approach, involving only energy conservation and leading therefore to the least biased distribution. If only statistics is involved, all possible states of the fragments that correspond to a given internal energy E will be populated with equal probability. These different states correspond to all possible partitions of the available energy E on the

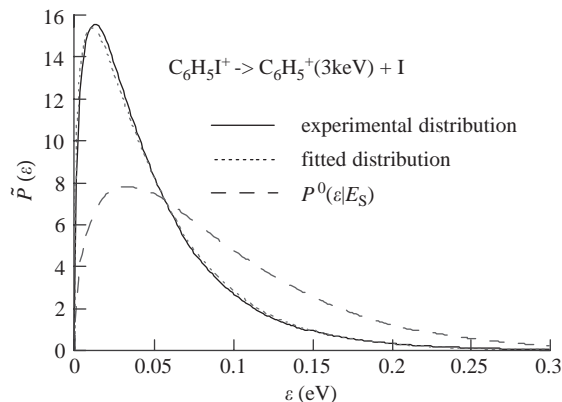


Figure 2

Kinetic energy release distribution for the metastable loss of iodine from the iodobenzene cation. Solid line: experimental. Dashed line: prior distribution (Eqn. (3)). Dotted line: fit to the maximum entropy distribution (see text).

degrees of freedom of the dissociated ion. Their total number is $\rho(E)$. Imagine that an energy ε has flown into the relative translational motion. The energy stored in the remaining degrees of freedom, i.e., the internal degrees of freedom of the fragments, is $E-\varepsilon$. Therefore the most statistical distribution function is given by:

$$P^0(\varepsilon|E) = \frac{\rho_t(\varepsilon) \rho_{\text{int}}(E-\varepsilon)}{\rho(E)} \quad (2)$$

and is referred to as the ‘‘prior distribution’’, indicated by the superscript zero. In Eqn. (2), $\rho_t(\varepsilon)$ is the density of translational states at relative kinetic energy ε . In other words, it is equal to the number of ways the translational energy can be partitioned among the three translational degrees of freedom. It is proportional to $\varepsilon^{1/2}$ (1, 6). $\rho_{\text{int}}(E-\varepsilon)$ is the density of states for the separated fragments. It represents the number of combinations generated by the different partitions of the energy $E-\varepsilon$ among the internal degrees of freedom of the fragments. Eqn. (2) can then be rewritten:

$$P^0(\varepsilon|E) = A(E) \varepsilon^{1/2} \rho_{\text{int}}(E-\varepsilon) \quad (3)$$

$A(E)$ ensures that the distribution is normalized to unity, i.e., $\int_0^E P^0(\varepsilon|E) d\varepsilon = 1$. Figure 2 also shows this

distribution calculated for the I loss reaction from ionized iodobenzene at the most probable internal energy sampled under the experimental conditions. The prior distribution reproduces the general Boltzmann-like shape of the experimental data but it is clearly wider. Such differences will be discussed and made use of later in the paper.

If, however, a reverse activation barrier is present, the situation differs somehow from the previous picture. Figure 3 shows a typical example: the distribution is shifted towards higher kinetic energies, indicating a preferred release of the reverse activation barrier as relative translational motion.

3. Experimental Determination of the Kinetic Energy Release Distribution of the Fragments

In order to determine experimentally the kinetic energy release distribution, $P(\varepsilon|E)$, for a given reaction, it is necessary to record the ion signal as a function of a parameter that depends on the relative translational energy of the fragments. In practice, the translational energy is monitored in the laboratory reference frame, whereas the required information is concerned with the center-of-mass frame, i.e., the reference frame linked with the dissociating molecular ion. When comparing different

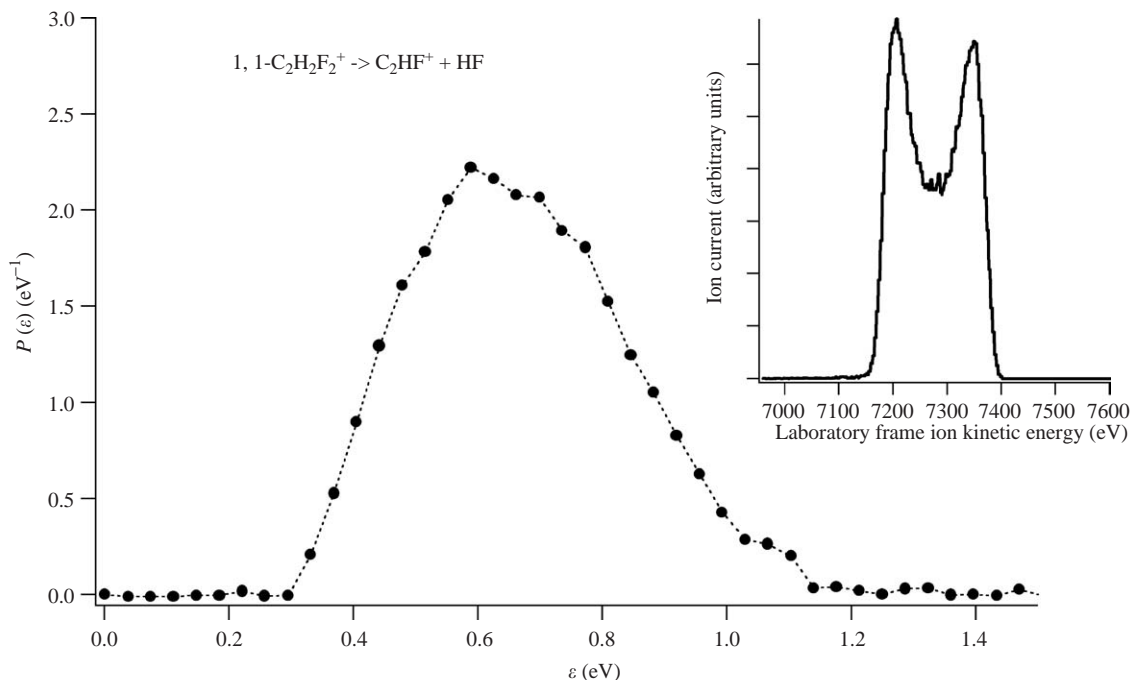


Figure 3

Kinetic energy release distribution for the metastable loss of HF from 1,1-difluoroethene cation: $\text{H}_2\text{CCF}_2^+ \rightarrow \text{HCCF}^+ + \text{HF}$. Inset: experimental peak profile in the laboratory frame.

experimental methods, three major criteria have to be considered.

(i) Ideally, the internal energy of the molecular ion, E , should be well defined. In practice, however, one deals with a more or less narrow distribution of internal energies, $T(E)$. The experimentally available KERD is then an average over $T(E)$:

$$\dot{P}(\varepsilon) = \int_{\varepsilon}^{+\infty} P(\varepsilon|E) T(E) dE \quad (4)$$

(ii) Translational energy resolution is the second critical point that determines the reliability of the KERD.

(iii) Angular discrimination effects are known to skew the distribution. When important amounts of translational energy are imparted to the fragments in directions perpendicular to the optical path of the spectrometer, these particles are severely deflected and usually not collected. Correction procedures have to be introduced then.

The advantages and drawbacks of three main experimental approaches will now be summarized.

3.1 Mass-analyzed Ion Kinetic Energy Spectroscopy (MIKES)

Such experiments are realized in a sector mass spectrometer consisting, in a minimal configuration, of a magnet followed by an electrostatic analyzer. Parent ions are accelerated in the ion source to a translational energy of a few kiloelectronvolts and then selected according to their mass-to-charge ratio by the magnet. They dissociate in the field-free region between the two sectors, either spontaneously or because of collisional activation, and the kinetic energy distribution of the ionic fragment is monitored in the laboratory frame by scanning the voltage across the plates of the electrostatic sector, hence the name mass-analyzed ion kinetic energy spectroscopy (see *Thermochemistry (Methods): The Correlation of Thermochemical Data*). As a result of the release of relative translational energy, the signal corresponding to a given fragment ion is broadened and the KERD, $\dot{P}(\varepsilon)$, has to be extracted from this broadened peak (7, 8). This technique has been mostly applied to study metastable dissociations (7), i.e., the dissociation of ions that possess an internal energy such that they dissociate spontaneously within the microsecond time scale, which is required for the ions to reach the field-free region. Note that such KERD determinations can also be performed on conventional geometry sector instruments, where the electrostatic analyzer is followed by the magnet, by scanning the source acceleration voltage, or by linked scanning of the magnetic field and of the field of the electrostatic analyzer. Let us now examine the three criteria mentioned above.

(i) Metastable ions are time-selected. As the rate constant depends on the internal energy, this time selection leads to an internal energy window. The latter is bell-shaped, slightly skewed and is given by the following equation:

$$T_j(E) = B(E) \frac{k_j(E)}{k(E)} \left[e^{-k(E)\tau_1} - e^{-k(E)\tau_2} \right] \\ \approx B(E)(\tau_2 - \tau_1)k_j(E)e^{-k(E)\bar{\tau}} \quad (5)$$

where $k(E) = \sum_j k_j(E)$ is the decay rate constant, $k_j(E)$ is the rate constant for the dissociation into the j -th channel, τ_1 and τ_2 are the entry and exit times of the dissociating ion in the field-free region, and $\bar{\tau} = \frac{\tau_1 + \tau_2}{2}$. $B(E)$ is a normalization constant. The width of $T(E)$ depends on how fast $k(E)$ increases with E . For the halogen loss from ionized halogenobenzene, it is typically in the 0.5–1.0 eV range. For the H₂ loss from ethylene or ethane ions, it is closer to 0.1 eV.

(ii) The translational energy resolution in such experiments is excellent. This results from the fact that the kinetic energy release, which can be as small as a few millielectron volts when considered in the center-of-mass frame, is much larger in the laboratory frame where the ion travels with a large (a few kiloelectron volts) translational energy. For a dissociation such as $m_1^+ \rightarrow m_2^+ + m_3$, the kinetic energy release in the molecular frame, ε , is related to the energy release in the laboratory frame, Δ , by the following equation (7):

$$\varepsilon = \frac{m_1^2}{4m_2m_3qV_{\text{acc}}} \Delta^2 \quad (6)$$

where q is the elementary charge ($q = 1.602 \cdot 10^{-19}$ C), and V_{acc} is the ion source acceleration voltage. This equation shows that the kinetic energy release in the laboratory frame is amplified compared to its value in the molecular frame by a factor related to the square root of the acceleration voltage. As an example, the metastable iodine loss from ionized iodobenzene, already considered, leads to an average kinetic energy release of about 50 meV, depending on the experimental conditions. If the molecular ion is accelerated to 8000 eV, the energy release in the laboratory frame will be equal to 50 eV. If the energy resolution of the electrostatic analyzer in the laboratory frame is set equal to 1 eV (resolving power = 8000), then the resolution in the center-of-mass frame will be 2 meV in this case.

(iii) For small kinetic energy releases, the KERD, $\dot{P}(\varepsilon)$, can be obtained by differentiating the Gaussian-like ion signal in the MIKE spectrum (laboratory frame) and by switching from variable Δ to ε (8). Such a simple procedure is not valid when discrimination effects are significant. This is particularly relevant in the presence of a large reverse activation barrier leading to substantial kinetic energy release. The peak shape in the MIKE spectrum is then dishd

(Fig. 3, inset). The fragment ion peak shape has to be fitted to a linear combination of basis functions corresponding each to a well-defined ε value. A basis function represents the peak shape that would be observed if only a single value of ε was released. The coefficients of the expansion of the peak profile on the basis functions give the KERD (9). As this procedure is relatively time-consuming, different simplified procedures have also been developed to handle this difficulty (10, 11).

3.2 Photoelectron–Photoion Coincidence Spectroscopy

This technique, known under the acronym PEPICO, has been developed to study the dissociation of internal energy-selected molecular ions (see *Ion Spectroscopy: Photoelectron Spectroscopy, Threshold Photoelectron Spectroscopy, and Pulsed Field Ionization*). The most useful version of this spectroscopy is the so-called threshold-PEPICO technique, which uses a variable wavelength photon source, e.g., synchrotron radiation, and where photoions are detected in delayed coincidence with zero-kinetic-energy electrons. Recent zero-kinetic energy techniques lead to resolutions better than 1 meV (see also *Ion Spectroscopy: Photoelectron Spectroscopy, Threshold Photoelectron Spectroscopy, and Pulsed Field Ionization*). The mass analyzer part of a PEPICO spectrometer is usually of the time-of-flight type (see *Instrumentation: TOF and RTOF*). As in the MIKES technique, the release of translational energy leads to a dispersion of velocities and thus of flight times, resulting in a broadening of the fragment ion peaks. The flight-time width, W , is related to the center-of-mass average kinetic energy release, $\langle\varepsilon\rangle$, by the following equation (12):

$$\langle\varepsilon\rangle = \frac{3}{16\ln 2} \frac{m_1}{m_2 m_3} (qE_{\text{acc}})^2 W^2 - \frac{m_2}{m_3} \langle E_{\text{th}} \rangle \quad (7)$$

in which q is the elementary charge and E_{acc} is the extraction field of typically a few to a few tens of V cm^{-1} . $\langle E_{\text{th}} \rangle$ is the average thermal energy of the parent ion. To extract the KERD, the time-of-flight peak shape is fitted to a linear combination of basis functions, as in MIKE spectroscopy (13).

The major advantage of this experimental approach is the excellent internal energy resolution. The major drawback is the poorer kinetic energy resolution. Compared with the MIKE spectrum, the amplification factor is smaller, because of the limited extraction field: compare Eqns. (6) and (7). As a consequence, the influence of the parent ion thermal energy is not negligible and deconvolution cannot be avoided.

Discrimination effects can be severe at higher ε values, especially with the moderate acceleration

fields required to maintain a good internal energy resolution. They must be taken into account in the basis functions.

On the whole, the time-of-flight threshold-PEPICO approach gives access to KERDs of lower quality than MIKES but with a very good energy selection. For such experiments, it is sensible to trust mainly the first moment of the distribution, i.e., the average kinetic energy release $\langle\varepsilon\rangle$.

3.3 Retarding Field Translational Ion Spectroscopy

In this technique (14), ions are produced by photoionization at fixed wavelength, using mainly a rare gas discharge lamp. Various resonance lines can be used, e.g., HeI (21.21 eV), NeI (16.67 eV and 16.85 eV), ArII (13.47 eV). The ions are submitted to a retarding field within the ionization chamber before they enter a quadrupole mass analyzer. As the retarding potential is scanned upwards, ions of increasing kinetic energy are prevented from reaching the detector. This generates an ion retarding potential curve from which the KERD can be extracted by numerical differentiation associated with a procedure correcting for angular discrimination effects. A correction procedure has been validated on the basis of ion trajectory simulations (15).

The kinetic energy resolution is limited by the thermal energy of the parent ion. For small KER values, this requires a deconvolution procedure. For this purpose, the retarding field spectrum of the parent ion is taken as the apparatus function.

The internal energy range sampled in this kind of experiment is wide, but known, ranging from the dissociation threshold up to the energy of the resonance line. The internal energy distribution sampled for a given dissociation process is given by the photoelectron spectrum recorded with the same resonance line multiplied by the branching ratio for the dissociation channel investigated.

4. The Average Kinetic Energy Release

The average kinetic energy release already provides useful global information, which can be used in ion thermochemistry and as a diagnostic tool for ion structural analysis. In the early days of MIKES, a conventional $\varepsilon_{0.5}$ (often denoted as $T_{0.5}$) value was defined by inserting the half-width of the metastable peak into Eqn. (6). Although quite arbitrary, this simple definition provided a reference value that could be used to distinguish, e.g., the dissociation of two isomeric ions. For a pure Gaussian MIKE profile, $\varepsilon_{0.5}$ is related to the average KER, $\langle\varepsilon\rangle$:

$$\langle\varepsilon\rangle = 2.16 \varepsilon_{0.5} \quad (8)$$

As the experimental peak profiles are rarely purely Gaussian, deviations from this relation are frequent. Today, the best way to obtain $\langle \varepsilon \rangle$ consists of first determining the full distribution and then calculating the average KER, i.e., its first moment, which is a very robust quantity:

$$\langle \varepsilon \rangle_E = \int_0^E \varepsilon P(\varepsilon|E) d\varepsilon \quad (9)$$

To illustrate the use of the average KER to distinguish between isomeric ions, we shall consider three examples involving small organic ions. Let us start with the two following isomers, $\text{CH}_3\text{CH}_2\text{OCH}_2^+$ and $\text{CH}_3\text{CHOCH}_3^+$, which can both fragment by metastable loss of H_2O and C_2H_4 (16). For $\text{CH}_3\text{CHOCH}_3^+$, both fragmentation channels have the same appearance energy. The average KER for the C_2H_4 loss from $\text{CH}_3\text{CH}_2\text{OCH}_2^+$ is equal to 17 meV. For $\text{CH}_3\text{CHOCH}_3^+$, $\langle \varepsilon \rangle$ is equal to 56 meV. For the water loss, these two values become 43 meV and 69 meV, respectively. The average KER is thus systematically larger for the $\text{CH}_3\text{CHOCH}_3^+$ precursor. The simple evaluation of $\langle \varepsilon \rangle$ thus allows us to distinguish between the isomers. From a mechanistic point of view, these data can be interpreted by a two-step dissociation for $\text{CH}_3\text{CHOCH}_3^+$: a slow H-shift leads to $\text{CH}_3\text{CH}_2\text{OCH}_2^+$, which then dissociates rapidly. The isomerization barrier lies higher than the dissociation asymptote.

The isomerization and dissociation chemistry of six different isomers of $\text{C}_5\text{H}_9\text{O}^+$ ions has been recently investigated (17). The three lowest energy structures are: $\text{CH}_3\text{CH}=\text{CH}-\text{C}^+(\text{H})\text{OCH}_3$, denoted (1) in the following, $\text{CH}_2=\text{CH}-\text{C}^+(\text{CH}_3)\text{OCH}_3$ (2) and $\text{CH}_2=\text{C}(\text{CH}_3)-\text{C}^+(\text{H})\text{OCH}_3$ (3). The major dissociation channel for these three ions in the metastable window is the loss of formaldehyde (H_2CO) with a branching ratio of about 0.75. Collisional activation experiments as well as isotope labeling show that no facile interconversion takes place between the three species. Their metastable peaks are Gaussian-like and the average KER increases in the following sequence: (1) > (3) > (2).

Let us now turn to collisionally activated dissociations (CAD). Hydrocarbon isomeric ions are indistinguishable in many mass spectrometric experiments (electron impact ionization, collision-induced dissociations). It has been recently demonstrated that KER measurements may provide a solution in some instances. *s*- C_4H_9^+ ($\text{CH}_3\text{CH}_2\text{CHCH}_3^+$) ions behave differently from *t*- C_4H_9^+ ions ($(\text{CH}_3)_3\text{C}^+$) when they lose CH_3 upon collisional activation with O_2 (18). In the former case, the average KER is equal to 500 meV—a flat-topped peak is observed—whereas it reaches only 90 meV in the latter case. This diagnostic behavior does not show up when He is the target gas. This is interpreted as reflecting the

non-Franck-Condon character of the collisional activation process.

Another structural application of the average kinetic energy release is concerned with the structure of large doubly charged molecular ions (19) (see also *Collisional Activation and Dissociation: Multiply Charged Ions*). Because of the Coulomb law, a charge separation reaction is associated with an asymptotic repulsive potential and with a large kinetic energy release. From the value of the average KER and from the known internuclear distance dependence of the Coulomb potential, an estimate of the intercharge distance can be deduced. This information provides clues about how flexible or rigid the molecular chain being investigated is.

As far as the mechanism of a chemical dissociation is concerned, it is enlightening to examine how the average KER varies with increasing internal energy. Different statistical approaches have been developed to calculate this variation. One recent approach is based on the maximum entropy method (20) and we delay its discussion until we have presented the basics of this formalism. A popular formula has been derived by Klots (1, 5, 21). The idea behind Klots' formula is that, for a large enough molecular ion, the number of internal degrees of freedom of the fragments is sufficient to compare this set of oscillators and rotators to an energy bath in equilibrium with the reaction coordinate. This bath is then characterized by an effective temperature T^* . This procedure amounts to replacing a microcanonical equilibrium, which is strictly speaking the appropriate model, by a canonical equilibrium. This is sensible only if the bath size is large enough. Considering the reaction coordinate as a very low frequency vibration leads to:

$$\langle \varepsilon \rangle = kT^* \quad (10)$$

According to statistical thermodynamics relationships, we may also write:

$$E = kT^* + \frac{r-1}{2}kT^* + \sum_{i=1}^s \frac{hv_i}{\exp\left(\frac{hv_i}{kT^*}\right) - 1} \quad (11)$$

where r is the number of fragment rotors. s is the number of vibrational degrees of freedom of the fragments, each of them being characterized by its normal frequency ν_i . From these two equations, it is possible to calculate numerically $\langle \varepsilon \rangle$ vs. E (Fig. 4). At high kinetic energies, i.e., at high effective temperatures, vibrations behave classically and $\langle \varepsilon \rangle$ becomes proportional to E , a fact already recognized a long time ago by Haney and Franklin (22). The simple use of (10)–(11) makes it quite popular in detecting nonstatistical behavior in unimolecular dissociations. The F loss reaction from CH_3F^+ illustrates this point (23). At energies up to 1.5 eV above the threshold, the

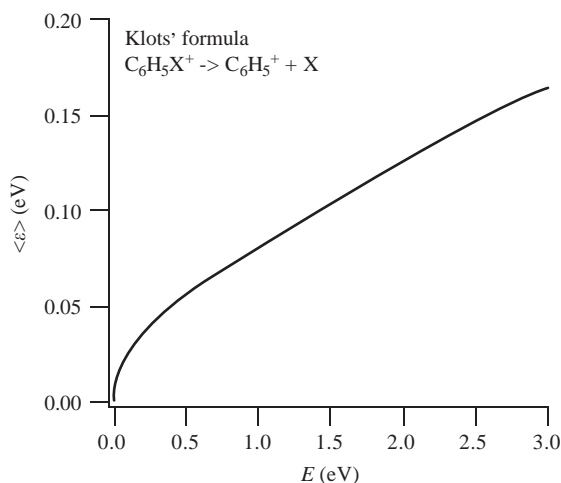


Figure 4
Relationship between the average kinetic energy release and the excess energy according to Klots' Eqn. (11) for a barrierless $C_6H_5X^+ \rightarrow C_6H_5^+ + X$ reaction.

measured average kinetic energy release agrees fairly well with the predictions of Eqns. (10)–(11). At $E = 1.5$ eV, $\langle \varepsilon \rangle$ increases suddenly and reaches values close to 90% release of the internal energy into relative translation. This behavior lasts up to $E = 2.5$ eV. After that, the average KER tends to level off. This nonstatistical behavior is thought to result from a fast direct decay along the repulsive potential energy surface of the \tilde{A} excited state. The transition from a statistical to an impulsive dissociation mechanism when switching from one electronic state to another one has been observed in a series of fluorobromomethane ions (24).

5. The Full Kinetic Energy Release Distribution (KERD): Survey of Statistical Models

The average kinetic energy release $\langle \varepsilon \rangle$ already provides us with useful information of structural and dynamical relevance. A more detailed analysis, however, requires consideration of the full distribution and confrontation with different theoretical models. When a Gaussian-like peak shape is observed in the laboratory frame, the resulting Boltzmann-like KERD is usually compared with a statistical calculation. One aims at getting some insight into the efficiency of intramolecular energy randomization. Different statistical variants exist. They are all based on the same general principle: all exit channels are equally probable provided the appropriate constants of motion are conserved. However, in order to implement this idea, specific ingredients have to be added. Let us briefly review them.

5.1 The RRKM Approach

According to the definition of the transition state, no energy transfer takes place once the associated critical hypersurface, which irreversibly separates the reactant from the fragments, has been crossed. The translational energy is assumed to arise entirely from the energy stored in the reaction coordinate. The KERD then reflects the energy partition at the transition state and is given by Eqn. (12).

$$P(\varepsilon|E) = \frac{\rho^\ddagger(E - E_0 - \varepsilon)}{N^\ddagger(E - E_0)} \quad (12)$$

E_0 is the zero-point energy of the transition state. $\rho^\ddagger(E - E_0 - \varepsilon)$ is the density of states of the transition state at energy $E - E_0 - \varepsilon$. $N^\ddagger(E - E_0)$ is the number of states of the transition state whose energy is smaller than or equal to $E - E_0$. This distribution peaks at zero kinetic energy. It is not appropriate when there is no reverse activation barrier (loose transition states). For tight transition states, it does not behave properly at energies located between the thermochemical threshold and E_0 . Exit channel interactions and, for H atom loss reactions, tunneling result in nonzero probabilities in the range between 0 and E_0 . For these reasons, the use of Eqn. (12) is not recommended.

5.2 The Prior Distribution

We have already met this formulation. In the prior distribution, only one constant of motion is introduced: the total available energy E . Therefore, all states of the pair of fragments at total energy E are equally probable. Translational energy is released in the three space dimensions and the kinetic energy release distribution is given by Eqn. (3). As is observed for simple cleavage reactions, the distribution starts at zero and goes through a maximum at nonzero kinetic energy (Fig. 2). Although it is sometimes presented as a crude model, it is best to reserve its use for comparison purposes with the actual KERD (see Section 5.4 below).

5.3 Phase Space Theory

The various phase space approaches (25–32), as well as the Statistical Adiabatic Channel Model (SACM) (33), conserve energy and also include conservation of angular momentum. This latter point is not at all trivial, because it is governed by the way some bending vibrations—called transitional modes—convert into individual rotations of the fragments and into fragment orbital motion. In most real life cases, the necessary information is lacking. One must then rely on models describing the

interaction between the receding fragments, which are themselves treated as atoms or as spherical or linear rotors. The basic idea of phase space theory is to connect the observables associated with a dissociation reaction with the more readily available cross-section for the reverse process, i.e., recombination of the fragments, using the principle of microscopic reversibility. A more detailed presentation of phase space theory applied to dissociations occurring via orbiting (loose) transition states is presented later in this chapter.

5.4 The Maximum Entropy Approach

Another approach is based on information theory (34, 35). The strategy consists of comparing the experimental KERD with the least biased statistical estimate, i.e., the prior distribution. From this comparison, information can be extracted on the nature of the dynamical constraint(s) governing the dissociation as well as a quantitative estimate of the amount of phase space that is effectively sampled. In other words, this methodology allows us to tell how far away from microcanonical equilibrium the system is. The key concept of this approach is the maximum entropy principle: among all possible distributions that could reproduce the experimental data, the most reliable inference is that of maximum entropy taking the dynamical constraints into account.

5.5 Problems Linked to the Presence of a Reverse Activation Barrier

In the presence of a reverse activation barrier, the statistical approaches usually fail badly. The two contributions to the excess energy (i.e., the reverse barrier and the nonfixed energy) give rise to quite different energy disposals (36). Exit channel interactions, which are ignored in the statistical theories, play a central role in the partitioning of the reverse activation barrier. A substantial fraction of the reverse barrier potential often converts into relative translational energy in a nonstatistical way. Classical trajectories represent one appropriate approach to account for this behavior (37, 38). The maximum entropy formalism has also been applied to such situations (36, 39).

6. Phase Space Theory for Orbiting Transition States

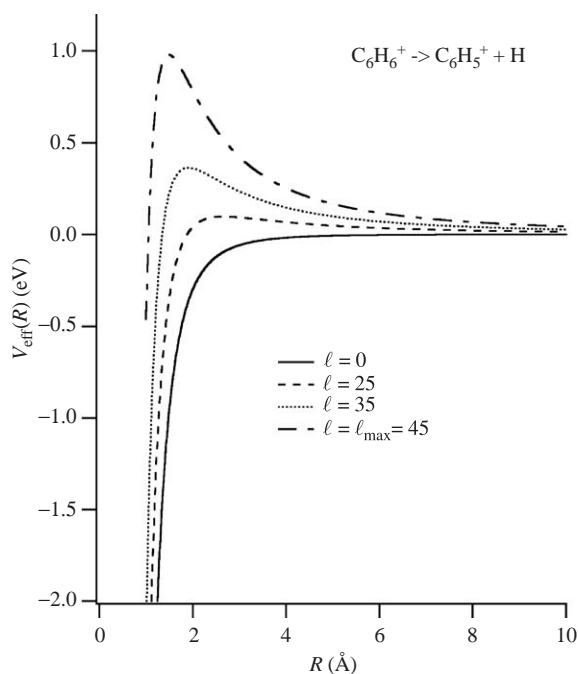
We now present, in more detail, phase space theory (PST), which is particularly suitable in the case of loose transition states in ionic dissociations, i.e., when the potential energy curve monotonously increases along the dissociation path. The key

advantage of this formalism is that angular momentum is explicitly taken into account. All decay channels are considered to be equally probable provided energy and angular momentum are conserved. The theory, initially developed by Light and Pechukas (25), has several variants resulting from the works of, in particular, Chesnavich and Bowers (26, 27, 28) and Klots (29, 30, 31). Phase space theory can be considered as the limiting case of a more general theory developed by Troe (31).

We consider a molecular ion with total angular momentum \mathbf{J} , which dissociates into fragments with rotational angular momentum \mathbf{j} and orbital angular momentum \mathbf{l} . This can be easily visualized for the dissociation of a linear triatomic species $ABC^+ \rightarrow AB^+ + C$ in a nondegenerate electronic state. J is the rotational quantum number of ABC^+ , j is the rotational quantum number of AB^+ , and l is the quantum number associated with the orbital motion of C around the center-of-mass of AB^+ . Note, however, that the mathematical derivation that will be outlined later in this section is not limited to this specific situation. Consider the recombination process, $AB^+ + C \rightarrow ABC^+$ and assume that the long-range potential between AB^+ and C is spherically symmetric. We may then integrate over the angular coordinates and, when this is done, we are left with an effective potential, $V_{\text{eff}}(R)$, which consists of two terms, an attractive contribution dominated by the ion-induced dipole term and a repulsive contribution, equal to $l(l+1)\hbar^2/2\mu R^2$ (μ is the reduced mass of the $AB^+ + C$ pair). A potential barrier, called the centrifugal barrier, results from these opposite contributions (Fig. 5) (see *Theory (Reactions): Ion-Molecule Collision Theory*). A so-called orbiting transition state (OTS) is then associated with the saddle point induced by this barrier. Note that OTS is an extremely loose transition state whose location is l -dependent. The phase space theory version that will be outlined here is based on the assumption that the energy partitioning at the orbiting transition state governs the product energy distributions. Most importantly, the orbiting energy at the transition state is adiabatically converted into fragment translational energy. In other words, l is assumed to be a good quantum number in the fragment region. To summarize, the orbiting transition state phase space theory makes the three basic assumptions:

- (i) the long-range potential is spherically symmetric;
- (ii) the orbiting transition state is located at the top of the centrifugal barrier; and
- (iii) orbital energy is adiabatically converted into fragment translational energy.

The kinetic energy release distribution of the fragments can be expressed as the rate constant for producing the fragments with translational energy ϵ and total angular momentum J divided by the total


Figure 5

Long range isotropic effective potential for the $C_6H_6^+ \rightarrow C_6H_5^+ + H$ reaction according to Eqn. (16). Three values of l are illustrated.

dissociation rate constant at given E and J :

$$P(\varepsilon|E, J) = \frac{k(\varepsilon, E, J)}{k(E, J)} \quad (13)$$

with $k(E, J) = \int k(\varepsilon, E, J) d\varepsilon$

The first key idea of phase space theory is to calculate the dissociation rate constant from the reverse, i.e., recombination, reaction, according to the microscopic reversibility—also called detailed balance—principle (6). This principle states that for a given process, $\alpha \rightarrow \beta$, the forward and reverse rate constants at energy E , $k_{\alpha\beta}$ and $k_{\beta\alpha}$, are related as follows:

$$k_{\alpha\beta} n_\alpha = k_{\beta\alpha} n_\beta \quad (14)$$

where n_α and n_β are the densities of states of the reactants (α) and the products (β) at total energy E . The dissociation rate constant can then be calculated provided the densities of states are known as well as the recombination rate constant. The second key idea of phase space theory applied to ionic dissociations is to use the Langevin capture cross-section (26–29) as the basic ingredient for calculating the rate. If $\sigma(j, \varepsilon \rightarrow J, E)$ denotes the recombination cross-section of fragments with a rotational angular momentum j colliding at translational energy ε to form the parent ion entity with total angular momentum J , then the corresponding

recombination rate constant can be written:

$$k_r(\varepsilon, j \rightarrow E, J) = \left(\frac{2\varepsilon}{\mu}\right)^{1/2} \sigma(j, \varepsilon \rightarrow J, E) \quad (15)$$

where the first term on the right side is the relative velocity of the fragments, v_{rel} .

Langevin theory is primarily concerned with the capture process between a structureless ion of charge equal to q and a structureless polarizable neutral particle (polarizability equal to α) at relative kinetic energy ε . The effective interaction potential is then equal to:

$$V_{\text{eff}}(R) = -\frac{\alpha q^2}{32\pi^2 \varepsilon_0^2 R^4} + \frac{l(l+1)\hbar^2}{2\mu R^2} \quad (16)$$

where ε_0 is the permittivity of vacuum ($\varepsilon_0 = 8.854 \times 10^{-12} \text{ Fm}^{-1}$) (see *Theory (Reactions): Ion–Molecule Collision Theory*).

The Langevin approach assumes that capture will take place when the relative kinetic energy is large enough for the colliding pair to overcome the centrifugal barrier. For a selected kinetic energy, this requires that l be smaller than $l_{\text{max}} = (1/\hbar)((\alpha q^2 \mu^2 \varepsilon)/(2\pi^2 \varepsilon_0^2))^{1/4}$. Stated in classical mechanics terms, only trajectories with an impact parameter b smaller than $b_{\text{max}} = l_{\text{max}}/(\mu v_{\text{rel}})$ will be captured. The Langevin cross-section is then equal to (26–29):

$$\sigma(j, \varepsilon \rightarrow J, E) = \frac{\pi \hbar^2}{2\mu \varepsilon} \sum_{l=0}^{l_{\text{max}}} (2l+1) P(j, l \rightarrow J) \quad (17)$$

$P(j, l \rightarrow J)$ is the probability that j and l combine to yield the total angular momentum J . Now, what we are actually interested in is not the recombination cross-section for fragments in a given (j, ε) state. In fact, we only want to specify the total fragment rotational energy, E_r , and, of course, the relative translational energy, ε . If j and l are supposed to vary continuously, Eqn. (17) becomes:

$$\begin{aligned} \sigma(E_r, \varepsilon \rightarrow J, E) &= \frac{\pi \hbar^2}{2\mu \varepsilon} \iint dl dj \rho(E_r, j) \\ &= \frac{\pi \hbar^2}{2\mu \varepsilon} \rho_{\text{ro}}(E_r, \varepsilon, J) \end{aligned} \quad (18)$$

If only one fragment can rotate, as in the $AB^+ + C$ case, j is the rotational quantum number of AB^+ and, in the classical limit, $E_r = B j^2$, where B is the rotational constant. In Eqn. (18), $\rho(E_r, j)$ is the rotational density of states of the pair of fragments whereas $\rho_{\text{ro}}(E_r, \varepsilon, J)$ corresponds to the rotational-orbital density of states, because it results from an integration over both the rotational quantum number j and the orbital quantum number l . The precise expression for $\rho(E_r, j)$ depends on the nature of the

fragments and can be inferred from tables provided in the literature (1, 26) for several situations: linear rotor + atom, spherical rotor + atom, two linear rotors, etc. The integration in Eqn. (18) has to be performed over the portion of the (j, l) space where the following conditions are fulfilled.

(i) l and j have to combine to J . This requires that

$$|J - j| \leq l \leq J + j \quad (19)$$

(ii) l cannot exceed l_{\max} defined earlier.

(iii) j cannot exceed j_{\max} according to total energy conservation: $E_r < E - \varepsilon$.

These conditions are usually summarized in the diagram shown in Fig. 6, where the shaded area corresponds to the allowed (j, l) space.

Basically, $\rho_{ro}(E_r, \varepsilon, J)$ in Eqn. (18) involves a simple counting of all possible rotational (j) and orbital (l) states of the orbiting transition state that can lead to a pair of fragments with the appropriate J , E_r , and ε values. The crux of the matter is that the orbital energy of the transition state is converted into relative translational energy of the fragments. The interplay between l and j imposed by the quantum mechanical angular momentum coupling rules leads to the essential consequence that rotation may no longer be separated from relative translation as was the case in the RRKM theory and for the prior distribution (see Eqns. (3) and (12) above).

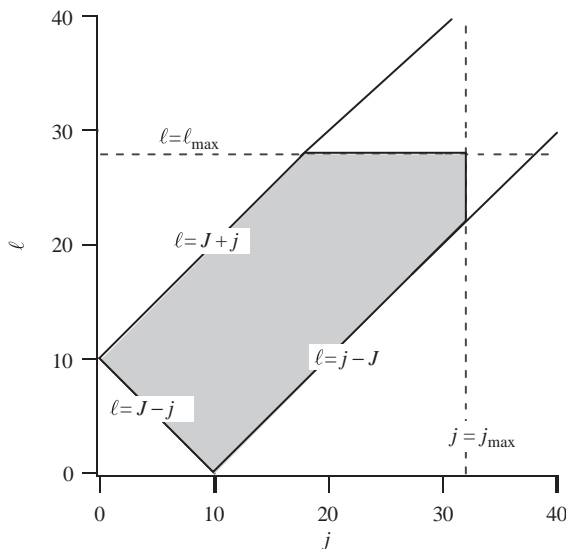


Figure 6

l - j coupling in a recombination process, at relative translational energy ε , into a species with total angular momentum J . The shaded area represents the allowed (l, j) space (see text). The maximum value of j is governed by energy conservation. The maximum value of l is determined by the relative translational energy.

The previous, somewhat lengthy discussion allows us now to calculate what we really need, i.e., $k(\varepsilon, E, J)$. From the microscopic reversibility Eqn. (14), it follows that:

$$k(\varepsilon, E, J) = \frac{g_{\text{frag}}(J)}{\rho_{\text{react}}(E, J)} \times \int_{E_r^{\min}}^{E-\varepsilon} k_r(\varepsilon, E_r \rightarrow E, J) \rho_t(\varepsilon) \rho_{\text{vib}}(E - E_r - \varepsilon) dE_r \quad (20)$$

where ρ_t and ρ_{vib} are, respectively, the translational and vibrational density of states of the fragments. $\rho_{\text{react}}(E, J)$ is the vibrational density of states of the reactant and $g_{\text{frag}}(J)$ is the rotational degeneracy. The rotational density of states of the fragments is hidden in k_r (see Eqns. (15) and (18)). The integration over E_r is required as the rotational energy is not selected in a KERD measurement. The lower integration limit, E_r^{\min} , can be understood easily from Fig. 6. If l_{\max} is smaller than J , then a minimum value of j —and thus of E_r —is required to yield J upon coupling with l . If l_{\max} is larger than J , then $E_r^{\min} = 0$. Using Eqns. (15) and (18) and the expression for the translational density of states of the fragments per volume unit,

$$\rho_t(\varepsilon) = \frac{(2\mu)^{3/2} \varepsilon^{1/2}}{(2\pi)^2 \hbar^3} \quad (21)$$

we obtain the following result:

$$k(\varepsilon, E, J) = \frac{g_{\text{frag}}(J)}{h \rho_{\text{react}}(E, J)} \times \int_{E_r^{\min}}^{E-\varepsilon} \rho_{\text{vib}}(E - E_r - \varepsilon) \rho_{ro}(E_r, \varepsilon, J) dE_r \quad (22)$$

Finally, introducing (22) into (13) and replacing the denominator by a normalization constant $A(E, J)$, leads to the kinetic energy release distribution.

$$P(\varepsilon|E, J) = A(E, J) \times \int_{E_r^{\min}}^{E-\varepsilon} \rho_{\text{vib}}(E - E_r - \varepsilon) \rho_{ro}(E_r, \varepsilon, J) dE_r \quad (23)$$

Let us now compare the results of the three formalisms, Eqns. (3), (12), and (23). All three of them contain densities of states, a fact reflecting the statistical nature of these approaches: all allowed exit channels are *a priori* equally probable. What makes the three treatments different is the nature of the constants of motion that are accounted for. In the prior distribution, no transition state is introduced, or, what is in fact equivalent, it is assumed to be

shifted to an infinitely large value of the reaction coordinate. The only constant of motion introduced is the total energy. The translational density of states is logically assumed to be tridimensional, i.e., it varies as $\varepsilon^{f/2}$. The RRKM approach (Eqn. (12)) amounts to considering that the energy stored in the reaction coordinate at the transition state is converted into two-dimensional fragment translational energy. This two-dimensional motion results from the conservation of orbital angular momentum in the asymptotic region, where the interfragment potential can be considered as spherically symmetric. The energy partitioning at the transition state—normally a more or less tight transition state—therefore determines the kinetic energy release distribution. No translational density of states appears explicitly in Eqn. (12) as it is a constant for a translation constrained in a two-dimensional space. Equation (23) displays a few interesting features. The phase space theory/orbiting transition state (PST-OTS) approach locates the transition state at the maximum of the centrifugal barrier. J is explicitly conserved and l is considered to be conserved from this orbiting transition state up to the fragments. As already emphasized, the coupling scheme between l and j makes the rotational and translational motions interdependent. There is still another essential consequence of the conservation of l from the orbiting transition state. Like the prior distribution, the PST-OTS distribution starts at zero because, for each value of l , the kinetic energy released is at least equal to the centrifugal barrier.

Figure 7 compares the kinetic energy release distribution for the $\text{C}_6\text{H}_5\text{Br}^+ \rightarrow \text{C}_6\text{H}_5^+ + \text{Br}$ dissociation calculated using the prior formalism and the phase space theory approach for $J=0$. This is the simplest situation, which can be appropriate for photodissociation experiments but not in the case of ion-molecule reactions. In this particular case, the $l-j$

coupling scheme requires that $l=j$ (Eqn. (19)). This comparison illustrates the effect of the conservation of angular momentum. Because of the large mass and polarizability of the bromine atom, the long-range attractive potential dominates and the centrifugal barrier has only a minor influence, so that the KERD is only marginally depleted at small values of ε . Note that the phase space approach usually treats—as we did for Fig. 7—nonlinear rotors as spherical rotors, with an effective rotational constant equal to $(B_x B_y B_z)^{1/3}$, where B_x , B_y , and B_z are the rotational constants of the considered asymmetric top.

Klots has developed (21, 29–31, 40) a version of the orbiting transition state phase space theory based, as already mentioned, on a canonical interpretation of the energy bath associated with the vibrational degrees of freedom of the fragments. This leads to Eqn. (11). For a spherical rotor \rightarrow spherical rotor + atom dissociation with J equal or close to zero, he derived Eqn. (24), which can be written as formula (25) in the case of a Langevin long-range potential (40):

$$P(\varepsilon|T^*) = A(T^*) \exp\left(-\frac{\varepsilon}{kT^*}\right) \times \left[1 - \exp\left(-\frac{B \ell_{\max}^2}{kT^*}\right)\right] \quad (24)$$

$$P(\varepsilon|T^*) = A(T^*) \exp\left(-\frac{\varepsilon}{kT^*}\right) \times \left\{1 - \exp\left[-\frac{B}{\hbar^2 kT^*} \left(\frac{\alpha q^2 \mu^2 \varepsilon}{2 \pi^2 \varepsilon_0}\right)^{1/2}\right]\right\} \quad (25)$$

$A(T^*)$ is as usually a normalization factor. When centrifugal effects do not dominate, relations (24) or (25), used together with Eqn. (11), provide us with an easy-to-handle alternative to Eqn. (23). The comparison is illustrated in Fig. 7. For ε values close to zero, (25) reduces to $P(\varepsilon|T^*) \propto \varepsilon^{1/2} \exp(-\varepsilon/kT^*)$ and contains therefore the same $\varepsilon^{1/2}$ increasing factor as the prior distribution.

As already alluded to, the consequences of angular momentum conservation are very dependent on the mass and on the polarizability of the neutral fragment. In the case of a light nonpolarizable atom such as hydrogen, the repulsive contribution of the effective potential dominates and leads to a severe depletion of the kinetic energy release distribution at small values of ε . This is illustrated in Fig. 8. For dissociations via loose transition states, it is generally observed that the kinetic energy release distributions are Boltzmann-like and can accordingly be fitted to the empirical form $\varepsilon^n \exp(-\beta\varepsilon)$ with $0 \leq n \leq 1$. For the iodine loss in Fig. 8, $n=0.13$ whereas $n=0.90$ for the H loss. These observations provide a rationale for Klots' so-called "model free approach" (41), which uses precisely this generalized Maxwell-Boltzmann relation. For highly polarizable fragments, the effect

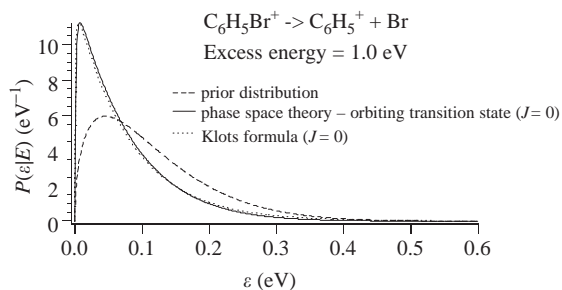


Figure 7

Calculated kinetic energy release distributions for the $\text{C}_6\text{H}_5\text{Br}^+ \rightarrow \text{C}_6\text{H}_5^+ + \text{Br}$ reaction at excess energy $E = 1$ eV. Dashed line: prior distribution. Solid line: PST-OTS distribution for $J=0$ according to Eqn. (23). Dotted line: distribution calculated for $J=0$ using Eqn. (25).

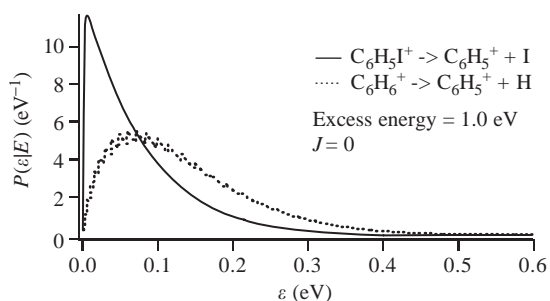


Figure 8

Kinetic energy release distributions for the $C_6H_5I^+ \rightarrow C_6H_5^+ + I$ (solid line) and $C_6H_6^+ \rightarrow C_6H_5^+ + H$ (dotted line) reactions, calculated by PST-OTS ($J=0$) at excess energy $E=1$ eV. For the H loss reaction, the l structure of the distribution is clearly visible, a result of the large centrifugal barriers.

of the centrifugal barrier is nearly vanishing and n is close to zero, a situation that can be described as a “two-dimensional Boltzmann distribution”. For H loss reactions, n is close to 1: this corresponds formally to a four-dimensional distribution. For fullerenes, Lifshitz found values close to 0.5 (5, 42) (see *Solvation and Clusters: Covalent Clusters of Group 14 Elements*).

7. Applications of Phase Space Theory

Phase space theory has been used as an extremely popular predictive or comparative tool to analyze both reaction rate constants and fragment energy distributions. For reactions without reverse activation barrier, the comparison of phase space predictions with the experimental data is often rewarding. A few recent examples include the dissociations of the bromo- and alkylbenzene cations (43–45). In the presence of a reverse barrier, it has been suggested that the kinetic energy release distribution should be written as the convolution of the respective contributions of the reverse barrier and of the nonfixed energy (i.e., the amount of energy in excess of the barrier). The latter is then evaluated using phase space theory and a deconvolution procedure yields the contribution of the reverse barrier (46).

Generally speaking, phase space theory suffers, of course, from the assumption of isotropic long-range forces. This weakness can be particularly stringent for the dissociation of strongly bound molecular species. For weakly bound noncovalent species, however, spherically symmetric long-range potentials are much more appropriate. Emphasis has been put in the last decade on the analysis of the fragmentations of van der Waals molecules and of clusters. An interesting application concerns the determination of binding energies. Fitting the observed kinetic energy release

distribution obtained by photodissociation to phase space theory makes the determination of the excess energy possible. This excess energy is then subtracted from the photon energy providing us with the required binding energy. An early example is the $N_2OH^+ \bullet OH + h\nu \rightarrow N_2OH^+ + OH$ reaction, which has been analyzed to yield a binding energy of 1.2 eV (47). For many clusters, however, the dissociation mechanisms can be complex, leading to at least bimodal distributions that cannot be modeled by the phase space formalism.

The analysis of the kinetic energy release distributions is instrumental to characterize organometallic ion–molecule reactions (48), such as $M^+ + C_nH_{2n+2} \rightarrow M^+(C_nH_{2n}) + H_2$, where M is a transition metal. Here again, fitting the observed kinetic energy distribution to the statistical phase space prediction leads to a determination of the bimolecular reaction enthalpy. From this result and from the known enthalpies of formation of the reactants and of H_2 , the bond energy in $M^+(C_nH_{2n})$ can be inferred. It must be mentioned here that for such bimolecular processes, a more sophisticated phase space formalism than the one outlined in this article is required. Three transition states are included in the calculations: two orbiting transition states corresponding to the entrance and the exit channels and a tight transition state governing the competition between the possible decay paths of the $M^+(C_nH_{2n+2})$ adduct: dissociating back to the reactants or evolving forward to the products.

Thermochemical information on clusters and fullerenes can be inferred from the analysis of kinetic energy distributions using Klots’ finite heat bath theory (49). The idea is to deduce the effective temperature T^* from a fit of the experimental data to Eqn. (24). This effective temperature is then related to the so-called isokinetic bath temperature via a formula involving the so-called Gspann parameter and the heat capacity. Trouton’s relation is then used to calculate the binding energy. Discussions can be found in the literature as to the most appropriate value for the Gspann constant. The uncertainty associated with this value is the major weakness of this approach. This methodology has been used extensively to analyze experiments involving fullerenes, including endohedral ones (see *Solvation and Clusters: Endohedral Complexes of Fullerenes and Mass Spectrometry*; *Solvation and Clusters: Covalent Clusters of Group 14 Elements*), and various ionized clusters (50, 51): carbon clusters, ammonia and xenon, negative cluster ions, rare gas clusters, etc. (see *Solvation and Clusters: Small Molecular Clusters*).

8. The Maximum Entropy Formalism: The Basic Ideas

The vantage point of the maximum entropy methodology is different from what has been described up

to now. Rather than trying to predict as well as one can the kinetic energy release distribution and then comparing it to the verdict of the experiment, the aim will be to quantify the discrepancies between the observed distribution and an appropriate prior expectation. The formalism is borrowed from information theory (34, 35). The basic idea can be expressed as follows. We observe the probability that an ion with total excess energy E will release a translational energy ε on the fragments upon dissociation. This defines a macrostate $(\varepsilon|E)$. If no dynamical constraint governs the dissociation, the energy partitioning will be dictated only by the number of microstates corresponding to the selected macrostate. The distribution corresponds then to the prior one, $P^0(\varepsilon|E)$, given by relation (3). This distribution is of maximum entropy as its information content is minimal. (Entropy is often referred to as the “missing information”). In real life, however, the dissociating ion travels through phase space regions where dynamical constraints operate and bias the energy partitioning. The maximum entropy formalism exploits the idea that among all of the distributions that reproduce the experimental data, the most unbiased choice is characterized by the largest entropy subject to the appropriate dynamical constraints. This maximum entropy distribution can be obtained by using the undetermined Lagrange multiplier technique.

In principle, the conservation of total angular momentum should be taken into account, so that the macrostate should be labeled $(\varepsilon|E, J)$. The most entropic distribution to consider as the starting point would then have to be that predicted by phase space theory (Eqn. (23)). However, phase space theory is fraught with uncertainties concerning the use of the Langevin model and hardly qualifies as an absolutely reliable starting point. Therefore, the prior distribution, which conserves only energy, has to be adopted (35). Energy conservation is straightforward, angular momentum is not, so that, at the present stage, the most secure and least biased approach is to take Eqn. (3) as the reference point.

The maximum entropy methodology can be summarized by the following sequential steps.

(i) Calculate the prior distribution, using Eqn. (3). This requires knowledge of the vibrational–rotational densities of states of the fragments.

(ii) Introduce the dynamical constraints. A dissociation process can be prevented from being fully statistical by the operation of one or possibly several physical parameters that strongly influence the dynamics. For translational energy released in the fragmentation of ions, it has been observed that the linear momentum of the separating fragments (which is proportional to the square root of the kinetic energy) is, as a rule, the appropriate constraint. This means that the actual KERD is related to the prior

distribution by the following equation:

$$P(\varepsilon|E) = e^{-\lambda_0} e^{-\lambda_1 \sqrt{\varepsilon}} P^0(\varepsilon|E) \quad (26)$$

where λ_0 and λ_1 are Lagrange multipliers whose function is to convert the prior distribution into the actual KERD.

Equation (26) suffices in most cases. In more complex situations, several constraints might operate and we might have to use a more complicated function such as:

$$P(\varepsilon|E) = e^{-\lambda_0} e^{-\lambda_1 \varepsilon^{n_1}} e^{-\lambda_2 \varepsilon^{n_2}} P^0(\varepsilon|E) \quad (27)$$

where n_1 and n_2 are appropriate powers.

(iii) Except when the parent ions are energy-selected, as in PIPECO experiments, it is necessary to average Eqns. (26) and (27) over the parent ion internal energy distribution $T(E)$ as expressed by Eqns. (4) and (5). The resulting equation is then fitted to the experimental data to determine the Lagrange parameters.

(iv) Compare the entropy of the actual distribution to that of the prior one. The general relation for the entropy of a continuous distribution $P(\varepsilon|E)$ is:

$$S(E) = - \int_0^E P(\varepsilon|E) \ln \left[\frac{P(\varepsilon|E)}{\rho(\varepsilon, E)} \right] d\varepsilon \quad (28)$$

$\rho(\varepsilon, E)$ is the density of states for a translational energy equal to ε and a fragment internal energy equal to $E-\varepsilon$ for the other degrees of freedom.

Inserting (26) or (27) and (3) into (28) leads to:

$$S(E) = S^0(E) + \lambda_0 + \lambda_1 \langle \varepsilon^{1/2} \rangle \quad (29)$$

or, possibly,

$$S(E) = S^0(E) + \lambda_0 + \lambda_1 \langle \varepsilon^{n_1} \rangle + \lambda_2 \langle \varepsilon^{n_2} \rangle + \dots \quad (30)$$

where $S^0(E)$ is the entropy of the prior distribution and $\langle \varepsilon^{1/2} \rangle$ is the average value of the constraint $\varepsilon^{1/2}$. The entropy deficiency with respect to the prior situation, $DS(E)$, is thus equal to:

$$DS(E) = S^0(E) - S(E) = -\lambda_0 - \lambda_1 \langle \varepsilon^{1/2} \rangle \quad (31)$$

By definition, DS is greater or equal to zero.

(v) The entropy deficiency is related to the fraction of fragment phase space that is effectively sampled, F :

$$F(E) = \exp[-DS(E)] \quad (32)$$

This approach makes therefore possible both the identification of the dynamical constraint(s) governing the dissociation process and a quantitative evaluation of its statistical character. In that sense, F has also been called an “ergodicity index”.

9. The Maximum Entropy Formalism: Applications

As far as the unimolecular dissociation of ions is concerned, the maximum entropy methodology outlined above has been applied mostly to simple bond cleavages. A detailed analysis of the halogen atom loss from ionized iodo-, bromo-, and chlorobenzene in the microsecond time range led to the conclusion that 70–80% of the energy accessible phase space was sampled (52). See again Fig. 2 for a comparison between the prior distribution, the experimental one and the fit of the latter to Eqn. (26) in the $C_6H_5I^+ \rightarrow C_6H_5^+ + I$ case. The missing 20–30% results from a dynamical constraint identified, as already mentioned, as the square root of the fragment relative kinetic energy, i.e., to the relative linear momentum. The associated Lagrange parameter, λ_1 , is positive, which means that less kinetic energy is released than *a priori* expected. This observation can be related to a quantum interpretation of the dissociation mechanism. Such bond cleavages can be understood as resulting from a vibrational predissociation, i.e., from a process where the energy initially deposited in optically active modes flows into dissociation modes because of anharmonic couplings. Stated in other, but equivalent words, the key quantity governing the energy flow process is the coupling between two kinds of states: those where the vibrational modes perpendicular to the reaction coordinate are highly excited and those associated with a large energy content in the reaction coordinate. This latter energy correlates with the relative translation energy of the fragments, ε . The coupling efficiency is found to decrease exponentially with the square root of ε . This coupling scheme has been investigated particularly in the case of the vibrational predissociation of van der Waals molecules, where it is known as the “momentum gap law” (53).

Does a reaction become less or more ergodic when internal energy is increased? This question has been investigated by the maximum entropy method (20, 54). For the bromine loss of ionized vinylbromide and for the iodine loss from the ethyliodide cation, the ergodicity index is found first to decrease and then to increase again (Fig. 9). This return to a statistical situation at higher internal energy can be linked to the nonselectivity of the ion preparation step. By either photoionization or electron impact, a collection of electronically excited states are initially populated, which then undergo rapid (10^{-14} s) internal conversions to the ground state via complex pathways. Only after this first step does dissociation take place. The nonadiabatic internal conversions lead to a multitude of initial conditions for the nuclear trajectories that explore phase space before dissociation. In addition, non-adiabaticity is synonymous with vibronic coupling, i.e., involves a strong tendency to randomize the

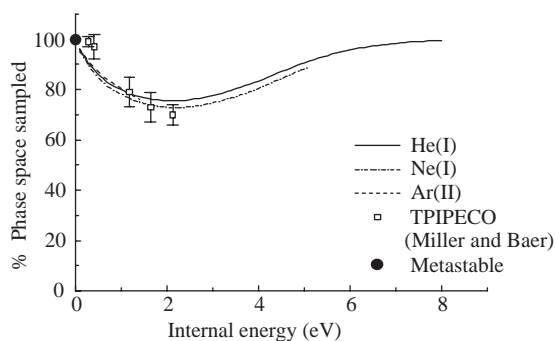


Figure 9

Fraction of sampled phase space as a function of the excess energy E . The experimental data from which this information is inferred have been obtained using the retarding field method with various resonance lines used to generate the ions: HeI (solid line), NeI (dashed-dotted line) and ArII (dashed line). The open symbols correspond to data derived from the TPIPECO work of Miller and Baer (55). The dot at $E \approx 0$ shows experimental results for metastable decomposition. Adapted from (54).

internal energy (see *Theory (Reactions): Non-adiabatic Reactions*).

Even if the full distribution is not known with high accuracy, some information can be inferred from the knowledge of the first moment, i.e., the average kinetic energy release. The following general relationship exists between the excess energy, the average kinetic energy release and the ergodicity index (20):

$$\frac{\langle \varepsilon \rangle}{E} = \frac{a}{b + \gamma} (1 + c e^{-DS}) \quad (33)$$

γ is the product of the excess energy E and the logarithmic derivative of the density of states at this energy. a , b , and c are constants related to the energy dependence of the density of states. If the latter increases as the exponential of $E^{1/2}$, then $a = 0.059$, $b = 0.48$ and $c = 1.85$. The fraction of phase space sampled can then be determined from a measurement of $\langle \varepsilon \rangle$ versus E , provided the density of states has been previously evaluated.

This approach is also promising for situations involving a reverse activation barrier. In this case, the excess energy has two origins: the reverse barrier (E_b) and the energy on top of this barrier ($E - E_b$), often called the nonfixed energy. Both will contribute to the observed kinetic energy release but with different probabilities. A simple additive scheme has been suggested (36):

$$\langle \varepsilon \rangle = a E_b + b(E - E_b) \quad (34)$$

Values of a of the order of 45–50% have been found by the maximum entropy method for the production of acyclic phenyl ions from protonated fluorobenzene and its perdeuterated analogue (39). Such high values are in keeping with data obtained for other systems and by other techniques. For the H_2 loss reaction from $CH_2NH_2^+$, $46 \pm 6\%$ of the reverse activation barrier is channeled into relative translation (38). An even larger value—about 75%—has been found for the H_2 loss from CH_2OH^+ (37).

10. Concluding Remarks

The analysis of the energy disposal in fragment ions, in particular the average kinetic energy release and the full kinetic energy release distribution, provides us with important clues concerning the reaction mechanism. The resulting information can be of different kinds:

(i) structure of either the reactant ion or the dissociation products;

(ii) thermochemistry of the dissociation process, from which binding energies can be inferred;

(iii) information on the statistical character of the reaction; in particular, the maximum entropy formalism leads to an ergodicity index $\exp(-DS)$ that measures the fraction of phase space effectively sampled by the fragments;

(iv) role of angular momentum conservation in the energy partitioning; the presently available models are, however, restricted to spherically symmetric long-range potentials and are thus particularly appropriate for the dissociation of weakly bound complexes. Clearly, additional work is required in this area to better take into account the role of transitional modes in the dissociation mechanism; and

(v) information on the partitioning of the reverse critical energy in elimination reactions involving a tight transition state; in such cases, the usual statistical models fail and alternative approaches are required.

Bibliography

- (1) Baer, T.; Hase, W. L. *Unimolecular Reaction Dynamics. Theory and Experiment*; Oxford University Press: New York, 1996.
- (2) Steinfeld, J. I.; Francisco, J. S.; Hase, W. L. *Chemical Kinetics and Dynamics*; Prentice Hall: Upper Saddle River, New Jersey, 1998.
- (3) Baer, T.; Mayer, P. M. Statistical Rice-Ramsperger-Kassel-Marcus Quasiequilibrium Theory Calculations in Mass Spectrometry. *J. Am. Soc. Mass Spectrom.* **1997**, *8*, 103–115.
- (4) Lorquet, J. C. Whither the Statistical Theory of Mass Spectra? *Mass Spectrom. Rev.* **1994**, *13*, 233–257.
- (5) Laskin, J.; Lifshitz, C. Kinetic Energy Release Distributions in Mass Spectrometry. *J. Mass Spectrom.* **2001**, *36*, 459–478.
- (6) Tolman, R. C. *The Principles of Statistical Mechanics*; Dover Publications: New York, 1979 (originally published by Oxford University Press, 1938).
- (7) Cooks, R. G.; Beynon, J. H.; Caprioli, R. M.; Lester, G. R. *Metastable Ions*; Elsevier Scientific Publishing: Amsterdam, 1973.
- (8) Holmes, J. L.; Osborne, A. D. Metastable Ion Studies (VIII): An Analytical Method for Deriving Kinetic Energy Release Distributions from Metastable Peaks. *Int. J. Mass Spectrom. Ion Phys.* **1977**, *23*, 189–200.
- (9) Rumpf, B. A.; Derrick, P. J. Determination of Translational Energy Release Distributions Through Analysis of Metastable Peaks. *Int. J. Mass Spectrom. Ion Processes* **1988**, *82*, 239–257.
- (10) Yeh, I. C.; Kim, M. S. Analysis of a Mass-analyzed Ion Kinetic Energy Profile. I. Analytical Expression for a Peak Shape at a Single Kinetic Energy Release. *Rapid Commun. Mass Spectrom.* **1992**, *6*, 115–120.
- (11) Szilágyi, Z.; Vékey, K. A Simple Algorithm for the Calculation of Kinetic Energy Release Distributions. *Eur. Mass Spectrom.* **1995**, *1*, 507–518.
- (12) Stockbauer, R. A Threshold Photoelectron–Photoion Coincidence Mass Spectrometer for Measuring Ion Kinetic Energy Release on Fragmentation. *Int. J. Mass Spectrom. Ion Phys.* **1977**, *25*, 89–101.
- (13) Mintz, D. M.; Baer, T. Kinetic Energy Release Distributions for the Dissociation of Internal Energy-selected CH_3I^+ and CD_3I^+ ions. *J. Chem. Phys.* **1976**, *65*, 2407–2415.
- (14) Loch, R.; Momigny, J.; Rühl, E.; Baumgärtel, H. A Mass Spectrometric Photoionization Study of CH_3F . The CH_2^+ , CH_3^+ and CH_2F^+ Ion Formation. *Chem. Phys.* **1987**, *117*, 305–313.
- (15) Hoxha, A.; Leyh, B.; Loch, R. Three-dimensional Kinetic Energy Distributions of Ions Using a Retarding Potential Analyzer. Analysis of Discrimination Effects by Ion Trajectory Simulations. *Rapid Commun. Mass Spectrom.* **1999**, *13*, 275–278.
- (16) Hvistendhal, G.; Williams, D. H. Energy Barrier to Symmetry-forbidden 1,3-Hydrogen Shifts in Simple Oxonium Ions. Metastable Peaks from Fast Dissociations. *J. Am. Chem. Soc.* **1975**, *97*, 3097–4101.
- (17) Bowen, R. D.; Heydorn, L. N.; Terlouw, J. K. The Chemistry of Some Low-energy $C_5H_5O^+$ Oxonium Ions. *Int. J. Mass Spectrom.* **2001**, *209*, 153–169.
- (18) Aubry, C.; Holmes, J. L. Butyl Cations and Their Gas-phase Dissociation Chemistry: Uniting Experiments with Theory. *J. Phys. Chem. A* **1998**, *102*, 6441–6447.
- (19) Szilágyi, Z.; Drahos, L.; Vékey, K. Conformation of Doubly Protonated Peptides Studied by Charge-separation Reactions in Mass Spectrometry. *J. Mass Spectrom.* **1997**, *32*, 689–696.
- (20) Lorquet, J. C. Unimolecular Reaction Dynamics from Kinetic Energy Release Distributions. 7. Average Translational Energy Release. *J. Phys. Chem. A* **2000**, *104*, 5422–5429.
- (21) Klots, C. E. Thermochemical and Kinetic Information from Metastable Decompositions of Ions. *J. Chem. Phys.* **1973**, *58*, 5364–5367.
- (22) Haney, M. A.; Franklin, J. L. Correlation of Excess Energies of Electron-impact Dissociations with the Translational Energies of the Products. *J. Chem. Phys.* **1968**, *48*, 4093–4097.

- (23) Weitzel, K. M.; Güthe, F.; Mähner, J.; Loch, R.; Baumgärtel, H. Statistical and Nonstatistical Reactions in Energy-selected Fluoromethane Ions. *Chem. Phys.* **1995**, *201*, 287–298.
- (24) Hatherly, P. A.; Smith, D. M.; Tuckett, R. P. Nonstatistical Effects in the Fragmentation of Electronic States of Gas-phase Polyatomic Molecular Ions. *Z. Phys. Chem. (München)* **1996**, *195*, 97–136.
- (25) Pechukas, P.; Light, J. C. On Detailed Balancing and Statistical Theories of Chemical Kinetics. *J. Chem. Phys.* **1965**, *42*, 3281–3291.
- (26) Chesnavich, W. J.; Bowers, M. T. Statistical Methods in Reaction Dynamics. In *Gas-phase Ion Chemistry*; Bowers, M. T., Ed.; Academic Press: New York, 1979; Volume 1, pp 119–151.
- (27) Chesnavich, W. J.; Bowers, M. T. Statistical Phase Space Theory of Polyatomic Systems. Application to the Unimolecular Reactions $C_6H_5CN^+ \rightarrow C_6H_5^+ + HCN$ and $C_4H_6^+ \rightarrow C_3H_3^+ + CH_3$. *J. Am. Chem. Soc.* **1977**, *99*, 1705–1711.
- (28) Chesnavich, W. J.; Bowers, M. T. Theory of Ion–Neutral Interactions: Application of Transition State Theory Concepts to Both Collisional and Reactive Properties of Simple Systems. In *Progress in Reaction Kinetics*; Jennings, K. R., Cundall, R. B., Eds.; Pergamon Press: Oxford, 1982; Volume 11, pp 137–267.
- (29) Klots, C. E. Kinetic Energy Distributions from Unimolecular Decay: Predictions of the Langevin Model. *J. Chem. Phys.* **1976**, *64*, 4269–4275.
- (30) Klots, C. E. The Reaction Coordinate and Its Limitation: An Experimental Perspective. *Acc. Chem. Res.* **1988**, *21*, 16–21.
- (31) Klots, C. E. Unimolecular Decomposition in a Spherically Symmetric Potential. *J. Chem. Phys.* **1993**, *98*, 1110–1115.
- (32) Troe, J. Specific Rate Constants $k(E, J)$ for Unimolecular Bond Fissions. *J. Chem. Phys.* **1983**, *79*, 6017–6029.
- (33) Quack, M.; Troe, J. Unimolecular Processes. IV. Product State Distributions after Dissociation. *Ber. Bunsenges. Phys. Chem.* **1975**, *79*, 469–475.
- (34) Levine, R. D.; Bernstein, R. B. Thermodynamic Approach to Collision Processes. In *Dynamics of Molecular Collisions (Part B)*; Miller, W. H., Ed.; Plenum Press: New York, 1976, pp 323–364.
- (35) Levine, R. D.; Kinsey, J. L. Information-theoretic Approach: Application to Molecular Collisions. In *Atom–Molecule Collision Theory. A Guide for the Experimentalist*; Bernstein, R. B., Ed.; Plenum Press: New York, 1979, pp 693–750.
- (36) Zamir, E.; Levine, R. D. Energy Disposal in Unimolecular Elimination Reactions. *Chem. Phys.* **1980**, *52*, 253–268.
- (37) Lee, T. G.; Kim, M. S.; Park, S. C. Partitioning of the Nonfixed Excess Energy and the Reverse Critical Energy in $CH_2OH^+ \rightarrow CHO^+ + H_2$: A Classical Trajectory Study. *J. Chem. Phys.* **1996**, *104*, 5472–5478.
- (38) Choi, T. H.; Park, S. T.; Kim, M. S. Theoretical and Experimental Studies of the Dissociation Dynamics of Methaniminium Cation, $CH_2NH_2^+ \rightarrow CHNH^+ + H_2$: Reaction Path Bifurcation. *J. Chem. Phys.* **2001**, *114*, 6051–6057.
- (39) Lorquet, J. C.; Lorquet, A. J. Unimolecular Reaction Dynamics from Kinetic Energy Release Distributions. 8. Protonated Fluorobenzene and Structure of the Phenyl Ion. *J. Phys. Chem. A* **2001**, *105*, 3719–3724.
- (40) Klots, C. E. Final State Distributions from Unimolecular Reactions: Implications of a General Theorem. *J. Phys. Chem.* **1995**, *99*, 1748–1753.
- (41) Klots, C. E. Kinetic Methods for Quantifying Magic. *Z. Phys. D* **1991**, *21*, 335–342.
- (42) Lifshitz, C. Unimolecular and Collision-induced Decomposition of Selected Cluster Ions. In *Cluster Ions*; Ng, C. Y., Baer, T., Powis, I., Eds.; Wiley: Chichester, 1993, pp 121–164.
- (43) Lim, S.-H.; Choe, J. C.; Kim, M. S. $C_6H_5Br^+ \rightarrow C_6H_5^+ + Br^+$ Occurs via Orbiting Transitions State. *J. Phys. Chem. A* **1998**, *102*, 7375–7381.
- (44) Hwang, W. G.; Moon, J. H.; Choe, J. C.; Kim, M. S. Dissociation Dynamics of *n*-Propylbenzene Molecular Ion. *J. Phys. Chem. A* **1998**, *102*, 7512–7518.
- (45) Kim, H. Y.; Choe, J. C.; Kim, M. S. Unimolecular and Photoinduced Dissociations of Aromatic $C_8H_{10}^+$ Molecular Ions. *J. Phys. Chem.* **2001**, *105*, 5751–5758.
- (46) Yeh, C.; Lee, T. G.; Kim, M. S. Determination of the Kinetic Energy Release Originating from the Reverse Critical Energy in Unimolecular Ion Dissociation. *Bull. Korean Chem. Soc.* **1994**, *15*, 241–245.
- (47) Graul, S. T.; Kim, H.-S.; Bowers, M. T. The Dynamics of Photodissociation of the Gas-phase $(N_2O \bullet H_2O)^+$ Cluster Ion. *Int. J. Mass Spectrom. Ion Processes* **1992**, *117*, 507–536.
- (48) van Koppen, P. A. M.; Bowers, M. T.; Haynes, C. L.; Armentrout, P. B. Reactions of Ground-State Ti^+ and V^+ with Propane: Factors That Govern C–H and C–C Bond Cleavage Product Branching Ratios. *J. Am. Chem. Soc.* **1998**, *120*, 5704–5712.
- (49) Klots, C. E. Kinetics in a Finite Heat Bath. In *Unimolecular and Bimolecular Reaction Dynamics*; Ng, C. Y., Baer, T., Powis, I., Eds.; Wiley: Chichester, 1994, pp 311–335.
- (50) Laskin, J.; Peres, T.; Khong, A.; Jiménez-Vásquez, H. A.; Cross, R. J.; Saunders, M.; Bethune, D. S.; de Vries, M. S.; Lifshitz, C. Mass Spectrometric Study of Unimolecular Decompositions of Endohedral Fullerenes. *Int. J. Mass Spectrom.* **1999**, *185/186/187*, 61–73.
- (51) Parajuli, R.; Matt, S.; Echt, O.; Stamatovic, A.; Scheier, P.; Märk, T. D. Decay Reactions of Rare Gas Cluster Ions: Kinetic Energy Release Distributions and Binding Energies. *Eur. Phys. J. D* **2001**, *16*, 69–72.
- (52) Urbain, P.; Leyh, B.; Remacle, F.; Lorquet, A. J.; Flammang, R.; Lorquet, J. C. Unimolecular Reaction Dynamics from Kinetic Energy Release Distributions. III. A Comparative Study of the Halogenobenzene Cations. *J. Chem. Phys.* **1999**, *110*, 2911–2921.
- (53) Ewing, G. E. Selection Rules for Vibrational Energy Transfer: Vibrational Predissociation of van der Waals Molecules. *J. Phys. Chem.* **1987**, *91*, 4662–4671.
- (54) Hoxha, A.; Loch, R.; Lorquet, A. J.; Lorquet, J. C.; Leyh, B. Unimolecular Dynamics from Kinetic Energy Release Distributions. V. How Does the Efficiency of Phase Space Sampling Vary with Internal Energy? *J. Chem. Phys.* **1999**, *111*, 9259–9266.
- (55) Miller, B. E.; Baer, T. Kinetic Energy Release Distribution in the Fragmentation of Energy-selected Vinyl- and Ethylbromide Ions. *Chem. Phys.* **1984**, *85*, 39–45.

B. Leyh* and J. C. Lorquet
Université de Liège, Belgium

*Research associate of the F.N.R.S. (Belgium)